Available online at www.sciencedirect.com
ScienceDirect
Nuclear Physics B Proceedings Supplement 00 (2014) 1–7
Nuclear Physics B Proceedings Supplement

Measurement of the W boson mass with the D0 detector

Hengne Li[a,b]

[a] University of Virginia, Charlottesville, VA, USA
[b] On behalf of the D0 collaboration

Abstract

The precision of the W boson mass from direct measurements is currently the limiting factor in the precision examination of the SM through the comparison of the direct measured Higgs boson mass and the predicted one. We present the measurements of the W boson mass using 5 fb^{-1} of integrated luminosity collected with the D0 detector during Run II at the Fermilab Tevatron collider, yields $M_W = 80.375 \pm 0.023$ GeV, and a new world average of $M_W = 80.385 \pm 0.015$ GeV. We further present the expectation from the ongoing measurements using the full D0 Run II data set of about 10 fb^{-1}.

Keywords:

1. Introduction

The Standard Model (SM) predicts a relationship between the W boson mass and other parameters of electroweak theory, such as the masses of the top quark and the Higgs Boson. In this relationship, the W boson mass (M_W) receives radiative corrections from loops that contain top quarks and Higgs bosons. However, beyond SM, such as in supersymmetry, the radiative corrections to the M_W can also come from loops including supersymmetry particles, which can possibly give a total correction to M_W of 100 to 200 MeV. Therefore, improving the measurements of the M_W and the top quark mass (m_t) can give a precise examination of the SM. The examination can be either done through the comparison of the directly measured Higgs boson mass (M_H) with the SM predicted one using the measured M_W and m_t as inputs, or through the comparison of the directly measured M_W and SM predicted M_W using the measured m_t and M_H as inputs. If the disagreement is big, we can infer contributions from theories beyond SM, such as supersymmetry.

Figure 1 shows the comparison of the SM predicted M_W [1] and the directly measured M_W. The predicted W boson mass is $M_W = 80.358 \pm 0.008$ GeV. If we compare the predicted M_W with the directly measured W boson mass world average $M_W = 80.385 \pm 0.015$ GeV [2], we can find a 1.4σ difference, which is actually a good agreement. However, comparing the precisions from direct measurements (±15 MeV) and the SM prediction (±8 MeV), we can see the precision from direct measurements is a limiting factor in the examination. In order to further scrutinize the SM, for example if we expect to see a 2σ deviation, we will need to improve the directly measured M_W to a precision of ∼10 MeV. At the same time, in the SM prediction of the M_W, the experimental precision of m_t contributes 4.6 MeV to the total uncertainty [1], further improvements on the top quark mass measurements is also important in this precision test.

The D0 experiment collected in total ∼10 fb^{-1} integrated luminosity. The measurement of M_W using the first 1 fb^{-1} was published in 2009, resulting a person of $M_W = 80.401 \pm 0.043$ MeV [3]. The measurement using another 4.3 fb^{-1} was published in 2012, together with the first 1 fb^{-1} results, yields $M_W = 80.375 \pm 0.023$ GeV [4], and a new world average of $M_W = 80.385 \pm 0.015$ GeV. There are another ∼5 fb^{-1} data being analyzed. With the full D0 data set, the final

Email address: Hengne.Li@cern.ch (Hengne Li)

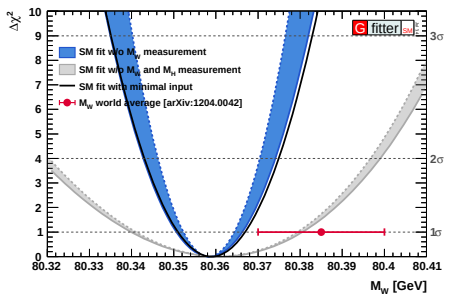

Figure 1: Comparison of the SM predicted M_W and directly measured M_W. The SM prediction is shown as the fitting $\Delta\chi^2$ versus M_W in blue band and grey band for cases with and without M_H measurements, respectively. In both cases, the direct measurements of M_W were excluded from the fit. The experimental world average of M_W is indicated by a dot with 1 σ error bars.

precision from D0 is expected to be 15 MeV.

In this proceedings, we take the published D0 measurements as example to present the analysis strategy. We will then discuss the expected precision from the ongoing full data set analysis, and the possible impacts.

2. Analysis strategy

We reconstruct two vector variables in the plane transverse to the beam direction from a $W \to e\nu$ event, namely, the electron transverse momentum ($\vec{p}_T^{\,e}$) and the transverse momentum of the hadronic recoil ($\vec{u}_T$) that balances the transverse momentum of the W boson.

The electron energy is reconstructed as a sum of the energies of calorimeter cells inside the electron reconstruction cone, while the direction of the electron is given by the track in the inner detector that matches spatially to the calorimeter cluster. The electron energy measurements are corrected for the energy loss due to uninstrumented material in front of the calorimeter. The correction is derived using detailed first-principle simulation. The material budget is determined from a fit to the longitudinal energy profile in the electromagnetic (EM) calorimeter. The gains of the readout cells of the EM calorimeter are calibrated using $Z \to ee$ events taking the world average Z boson mass [5] (M_Z) as reference.

The $\vec{u}_T$ is reconstructed by a vectorial sum of the transverse energies of all the calorimeter cells outside the electron reconstruction cone. The longitudinal component of the hadronic recoil cannot be determined due to the limited pseudorapidity coverage ($|\eta| < 4.2$) of the calorimeter. Therefore, the neutrino longitudinal momentum, which is required to reconstruct the invariant mass of the W boson, cannot be determined.

From $\vec{p}_T^{\,e}$ and $\vec{u}_T$, we can calculate three transverse observables for M_W extraction: the transverse mass of the W boson ($m_T = \sqrt{(p_T^e + \not{E}_T)^2 - (\vec{p}_T^{\,e} + \vec{\not{E}}_T)^2}$), the electron transverse momentum ($p_T^e = |\vec{p}_T^{\,e}|$), and the missing transverse energy ($\not{E}_T = |-\vec{p}_T^{\,e} - \vec{u}_T|$) due to the neutrino transverse momentum.

A fast Monte-Carlo (MC) model is developed to generate a series of templates for the above three observables based on different M_W hypotheses. The M_W is determined, specially for each observables, using a binned likelihood fit of the predicted templates to the data.

For the $W \to e\nu$ event selection, we require an electron in Central Calorimeter (CC) with $p_T^e > 25$ GeV. The event is required to satisfy $\not{E}_T > 25$ GeV, $u_T < 15$ GeV, and $50 < m_T < 200$ GeV. The requirement on u_T is made to constrain the transverse boost of the W boson, since the transverse boost of the W boson degrades the sharpness of the Jacobian edge in the p_T^e distribution. However, this treatment also translates certain uncertainties from the hadronic recoil modeling to the p_T^e. There are 1 677 394 candidate $W \to e\nu$ events after selection.

The $Z \to ee$ events are the control sample for tuning the fast MC, such as the electron energy scale and the hadronic recoil model. The $Z \to ee$ events are selected by requiring two electrons both with $p_T^e > 25$ GeV. Events are also required to have $u_T < 15$ GeV to constrain the transverse boost of the Z boson, and $70 < m_{ee} < 110$ GeV, where m_{ee} is the invariant mass of the electron pair. There are 54 512 $Z \to ee$ candidate events with both electrons in CC, which are used for most of the model tuning. Events allowing one electron in the Endcap Calorimeter (EC, with $1.5 < |\eta| < 2.5$) are only used for measurements of the electron reconstruction efficiency.

3. Fast Monte-Carlo model

The fast Monte-Carlo (MC) model for template generation has to simulate W and Z boson production and decay, the electron energy response, the hadronic recoil, the underlying events contamination, the electron reconstruction efficiency, and the background.

3.1. Boson production and decay

The boson production and decay are simulated using `RESBOS` [6] event generator combined with `PHOTOS` [7]. `RESBOS` is a next-to-leading order event generator including next-to-next-to-leading order logarithm resummation of soft gluons. `PHOTOS` generates up to two final state radiation (FSR) photons. Parton distribution

functions are described using CTEQ6.6 [8]. The boson transverse momentum prediction in RESBOS is dominantly determined by the nonperturbative parameter [9] g_2. The g_2 value [10] 0.68 ± 0.02 GeV^2 is used.

3.2. Electron energy response

The electron energy response is modeled by firstly modeling the energy responses that are not a linear function of the electron true energy. Then, we assume the rest of the energy response is a linear function of the electron true energy, fit to the $Z \to ee$ data sample to determine the scale.

The energy loss correction, as one of the non-linear energy responses, is applied to the data. There are also certain non-linear energy responses due to the high instantaneous luminosity to be modeled in the fast MC.

One of them is the reduction of EM calorimeter gain due to a high voltage (HV) drop caused by a large instantaneous pile-up energy deposition. A large current that flows through the resistive coat of the HV pads of calorimeter cells creates a reduction of the HV. The HV supplies are connected at both ends of the CC modules (at $|\eta| = 1.2$). Therefore, HV drop is larger for cells at small $|\eta|$ than for cells at large $|\eta|$. This gain loss is modeled as function of instantaneous luminosity and detector η in the fast MC. The EM calorimeter calibration at the cell level applied to the data is done in the absence of the knowledge of the HV drop. Certain imperfections in such a calibration are expected. Thus, an addition model of the residual miscalibration as a function of detector η is introduced in the fast MC.

Another non-linear energy response is understood as an effect of the electron reconstruction cone. The electron energy is reconstructed as a sum of energies deposited in a cone consisting of 13 calorimeter towers. Not only the electron deposits its energy into this cone, but also some of the hadronic recoil, pile-up, and spectator parton interactions. The energy deposition from the latter sources does not come from the true electron but is reconstructed as part of the electron energy in the data. This additional energy contribution is modeled in the fast MC as a function of instantaneous luminosity, η, $u_{\parallel}$ (the $\vec{u}_T$ projection to the electron direction), and SET (the scalar sum of the transverse energy deposited all over the calorimeter with cells in the electron reconstruction cone excluded).

After modeling of the non-linear responses, the linear response is modeled as $E = \alpha \cdot (E_{true} - 43\ \text{GeV}) + \beta + 43\ \text{GeV}$, where, α is the energy scale, β is the energy offset, and 43 GeV is an arbitrary offset introduced technically to improve the stability of the fit for α and β. The parameters α and β are determined by a template fit to the m_{ee} versus f_Z distribution of the $Z \to ee$ events, where $f_Z = (E_1 + E_2) \cdot (1 - \cos\omega)/m_{ee}$, E_1 and E_2 are energies of the two electrons, and ω is the opening angle between the two electrons. The α and β are determined separately for four instantaneous luminosity subsamples, and are consistent with each other, as shown in Figure 2 (c). After the electron energy scale tuning, a Z boson mass fit returns $M_Z = 91.193 \pm 0.017(\text{stat})$ GeV, which is in good agreement with the world average ($M_Z = 91.188$ GeV). The M_Z fit is shown in Figure 2 (a).

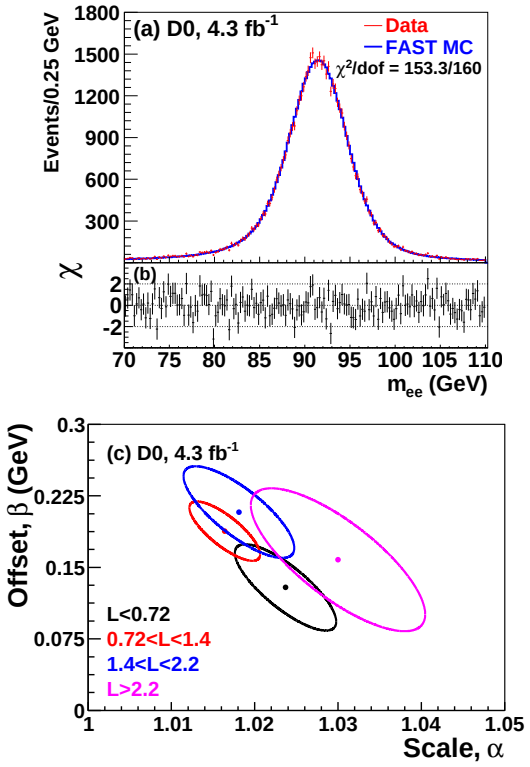

Figure 2: (a) The dielectron invariant mass distribution in $Z \to ee$ data and from the fast MC, (b) the χ plot of (a), and (c) the fitted scale and offset 1-sigma contours in bins of instantaneous luminosity (in units of $10^{32}\text{cm}^{-1}\text{s}^{-1}$).

3.3. Hadronic recoil

The hadronic recoil ($\vec{u}_T$) reconstructed from the data contains contributions from the hadrons recoiling against the W boson, and additional components that are (mostly) independent of the W boson boost. These additional components include spectator parton interactions, pile-up, a small part of all the components above that enter the electron reconstruction cone, and the FSR photons outside the electron reconstruction cone.

All these components are modeled separately in the fast MC, and a vectorial sum of them gives the $\vec{u}_T$. Free parameters are reserved to tune the recoil model. The hadronic response and resolution are tuned using the mean and width of the $\eta_{\rm imb}$ distributions, respectively, of the $Z \to ee$ events in bins of p_T^{ee}, where $\eta_{\rm imb}$ denotes the projection of the sum of the dielectron transverse momentum and $\vec{u}_T$ vectors on the axis bisecting the dielectron directions in the transverse plane [11].

3.4. Efficiency

The kinematic dependence of the electron reconstruction efficiency sculpts the distributions of the observables used to measure the M_W. The pile-up due to high instantaneous luminosity and the hadronic recoil are the two major sources that contaminate the electron reconstruction window and give inefficiency in the electron reconstruction. The effects of pile-up can indirectly introduce kinematic dependence of the efficiency. For instance, under a given pile-up contamination, a high energy electron can be more easily identified than a low energy electron. The hadronic recoil contamination depends on the amount of hadronic activity and also the relative orientation of the hadronic recoil with respect to the electron.

The kinematic dependence of the efficiency is determined and modeled in the fast MC in two steps. In the first step, we extract the efficiency dependence from a high statistics detailed `GEANT` [12] MC simulation (full MC) of the $W \to e\nu$ and $Z \to ee$ events generated using the `PYTHIA` [13] event generator, and model it in the fast MC. The full MC is overlaid at the cell level with a dedicated pile-up collider data sample which is weighted according to the instantaneous luminosity distribution (with random bunch crossings) of the data set used in this analysis. This step simplifies the modeling of the complicated correlations among the various efficiency dependencies with a data-based determination of the pile-up impacts. The second step is to extract the dependence of the efficiency on the major variables (p_T^e, $u_\parallel$, SET, instantaneous luminosity, etc.) from the data, and compare them with those from the full MC. Excellent agreement is found between the full MC and collider data.

3.5. Backgrounds

Backgrounds in the W boson candidate sample modify the shapes of the distributions of the three observables. The major backgrounds are $Z \to ee$ events where one of the electrons escapes detection, multijet events where a jet is misidentified as an electron with $\not\!\!E_T$ arising from misreconstruction, and $W \to \tau\nu \to e\nu\nu\nu$ events. The fractions of the backgrounds in the W boson candidate sample are 1.08% for $Z \to ee$, 1.02% for multijet events, and 1.67% for $W \to \tau\nu \to e\nu\nu\nu$ events. The impact of the uncertainties in the background model on the M_W measurement is found to be small.

3.6. Systematic uncertainties

The systematic uncertainties of the M_W measurements are listed in Table 1. They are divided into two categories: from experimental sources and from boson production and decay modeling.

Among the experimental aspects, the uncertainties from electron energy calibration, electron energy resolution model, and hadronic recoil model are driven by the limited statistics of the $Z \to ee$ control sample. The shower modeling systematic uncertainties reflect the uncertainties in the amount of uninstrumented material, and the energy loss systematic uncertainties arise from the finite precision of the simulation of electron showers based on a detailed model of the detector geometry. The systematic uncertainties of electron calibration, electron resolution, electron reconstruction efficiency, hadronic recoil model and backgrounds are determined by varying the corresponding parameters within the statistical uncertainties of their measurements.

The uncertainties due to boson production and decay modeling are dominantly due to the PDFs. In principle, the transverse observables used in the M_W measurement are insensitive to the uncertainties of the (longitudinal) PDFs. However, our requirements on the lepton pseudorapidity ($|\eta| < 1.05$) is not invariant under longitudinal boosts. Changes in the PDFs can modify the shapes of the transverse observables in the presence of the pseudorapidity requirements. The PDF uncertainties are propagated to M_W by generating ensembles of W boson events using `PYTHIA` with CTEQ6.1 [14]. The QED uncertainties are estimated by comparing `PHOTOS` to `WGRAD` [15] and `ZGRAD` [15] event generators, which provide a more complete treatment of electroweak corrections at the one radiated photon level. The uncertainties from boson transverse momentum modeling is determined by propagation of the uncertainty of the g_2 parameter.

4. Results from half of the D0 data set

The value of M_W is extracted by fitting templates of the three observables (m_T, p_T^e, and $\not\!\!E_T$) generated by the fast MC to the distributions from the collider data. The fitting results are shown in Table 2, together with optimized fit ranges, for the three observables. Figure 3

Source	ΔM_W (MeV) m_T	p_T^e	$\not\!\!E_T$
Electron energy calibration	16	17	16
Electron resolution model	2	2	3
Electron shower modeling	4	6	7
Electron energy loss model	4	4	4
Hadronic recoil model	5	6	14
Electron efficiencies	1	3	5
Backgrounds	2	2	2
Experimental subtotal	18	20	24
PDF	11	11	14
QED	7	7	9
Boson p_T	2	5	2
Production subtotal	13	14	17
Total	22	24	29

Table 1: Systematic uncertainties of the M_W measurement of the 4.3fb^{-1} data set [4].

shows the distributions of the three observables in data and the comparison with templates from fast MC for the best fit M_W. During the tuning of the fast MC to describe the collider data, an unknown constant offset is added to the M_W values returned from the fits, which is the same for the three observables. This enables the tuning of the fast MC to be done without the knowledge of the final results.

Variable	Fit Range (GeV)	M_W (GeV)
m_T	$65 < m_T < 90$	80.371 ± 0.013
p_T^e	$32 < p_T^e < 48$	80.343 ± 0.014
$\not\!\!E_T$	$32 < \not\!\!E_T < 48$	80.355 ± 0.015

Table 2: Results from the fits to data. The quoted uncertainty is solely due to the statistics of the W boson sample.

Combining the results from m_T and p_T^e methods using the BLUE [17] method, we obtain the final result of the 4.3 fb^{-1} measurement:

$$\begin{aligned} M_W &= 80.367 \pm 0.013 \text{ (stat.)} \pm 0.022 \text{ (syst.) GeV} \\ &= 80.367 \pm 0.026 \text{ GeV}. \end{aligned}$$

The result from the $\not\!\!E_T$ method is not used in the combination. In the combination, we assume 100% correlation for those uncertainties that are nonstatistical in nature, such as the QED uncertainties, to protect them from being decreased. However, with this protection, the BLUE combination gives a sizable negative weight for the M_W value from the $\not\!\!E_T$ method which has relatively larger uncertainties. The interpretation is that the

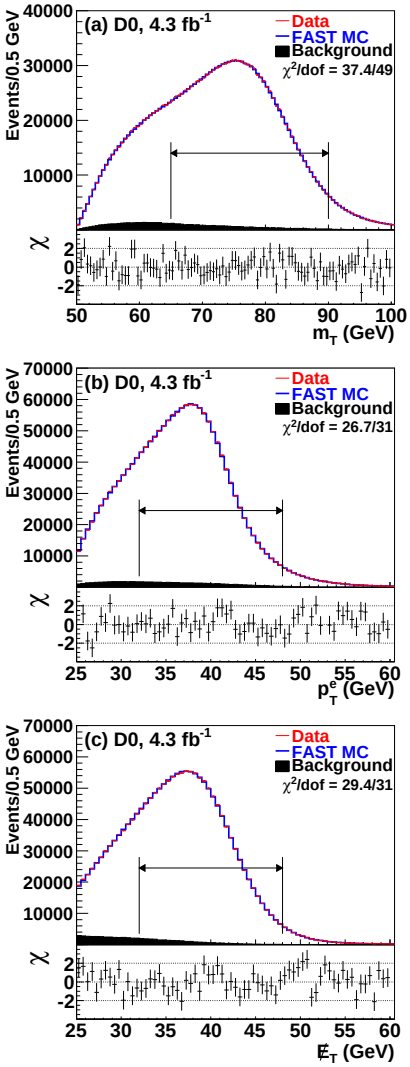

Figure 3: The (a) m_T, (b) p_T^e, and (c)$\not\!\!E_T$ distributions for data and fast MC simulation with backgrounds, together with the χ plots comparing data and fast MC. The fit ranges are indicated by the double-ended horizontal arrows.

central values of M_W from the other more precise methods (m_T and p_T^e) have also fluctuated apart from the true value of M_W in the same direction as the less precise $\not{E}_T$ method. Given that it is our protection that introduces the negative weight, and the contribution to the combined precision from the $\not{E}_T$ method is negligible, we decide to only use the m_T and p_T^e methods in the above combination to avoid the potential bias.

We combine our result with the earlier D0 measurement [4] to obtain the D0 5.3 fb^{-1} result:

$$\begin{aligned} M_W &= 80.375 \pm 0.011 \text{ (stat.)} \pm 0.020 \text{ (syst.) GeV} \\ &= 80.375 \pm 0.023 \text{ GeV}. \end{aligned}$$

The precision achieved is the same as the previous world average.

The combination with all previous measurements and the recent CDF measurement [18] gives the new world average [2]:

$$M_W = 80.385 \pm 0.015 \text{ GeV}.$$

This result, together with previous measurements, are summarized in Figure 4.

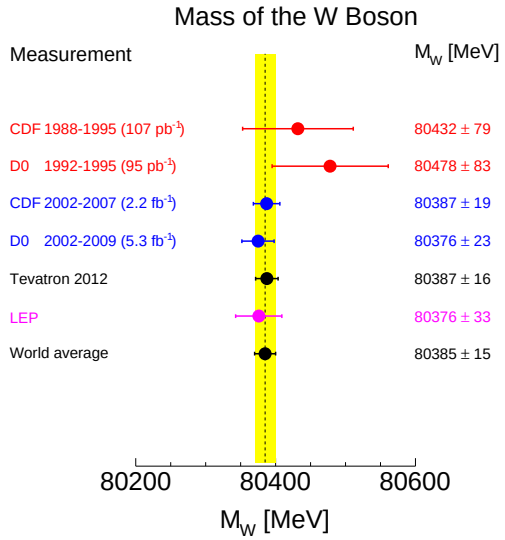

Figure 4: Summary of the measurements of the W boson mass and their average as of March 2012.

5. Projection to full D0 data set and outlook

The projection of the expected results using the 10 fb^{-1} D0 full data set is summarized on Table 3. The full data set analysis using only the CC electrons (as for the published measurements) is expected to give a 19 MeV precision on the M_W. If we include the EC electrons in the analysis, we could expect a final M_W precision of 15 MeV from D0 full data set.

Source (Unit in MeV)	CC	CC+EC
Statistical	9	8
Experimental syst.		
Electron energy scale	11	10
Electron resolution model	2	2
Electron showering modeling	2	2
Electron energy loss model	2	2
Hadronic recoil model	3	2
Electron efficiencies	1	1
Backgrounds	2	2
Experimental subtotal	12	11
Theoretical syst.		
PDF	11	5
QED	3	3
Boson p_T	2	2
Production subtotal	12	6
Systematic total	17	13
Total	19	15

Table 3: Projection of the uncertainties to the D0 10 fb^{-1} full data set. In which, "CC" refers to "Central Calorimeter", "EC" refers to "Endcap Calorimeter". The column labeled "CC" is the projected results using only W events with decay electrons fall in the CC, and that labeled "CC+EC" is the projected results using both CC and EC electrons.

In this projection, the expected improvements, besides larger data set, are the systematic uncertainties from the electron showering modeling (energy nonlinearity), electron energy loss modeling (the energy loss differences between electrons from W and Z bosons decay), and from theoretical modeling of the QED and the PDFs.

The systematic uncertainties of electron showering modeling and energy loss modeling, have not been updated since the 1 fb^{-1} analysis. Larger size of MC samples for electron showering and energy loss studies have been generated for reducing these two uncertainties. They are expected to be reduced from 4 MeV (Table 1) to 2 MeV (Table 3).

The QED uncertainties are similarly not having been revisited since the 1 fb^{-1} analysis. We are trying a different approach to address the QED uncertainties by comparing the RESBOS+PHOTOS modeling with the implementation of electroweak corrections [20] in the POWHEG BOX [19]. The QED uncertainties are expected to be reduced from 7 MeV (Table 1) to 3 MeV (Table 3).

The PDF uncertainties are expected to be largely reduced after including the EC electrons in the analysis. In principle, the transverse observables such as m_T, p_T^e, and $\not\!\!E_T$ are insensitive to the uncertainties in the PDF (function of longitudinal observable, i.e. the longitudinal momentum fraction). However, our cuts on the electron η ($|\eta| < 1.0$) to select the CC electrons is not invariant under longitudinal boosts. Changes in PDF can modify the shapes of the transverse observables under η cuts, thus, introduces the PDF uncertainties. Therefore, extending the η coverage such as including the EC electrons, can reduce the dependence of the transverse observables on the (longitudinal) PDF. A factor of two reduction of the PDF uncertainties is expected by including the EC electrons in the analysis.

Including the expected D0 full data set results, the corresponding new world averages would be ∼14 MeV and ∼12 MeV for CC and CC+EC scenarios, respectively. If the SM predicted M_W precision can also be improved by including more precisely measured m_t, and the central values of the predicted and the directly measured M_W did not change in the future, we could expect a 2σ difference. However, if we expect better discrimination, we need the contributions from other experiments such as CDF, ATLAS and CMS, and future electron-positron colliders such as ILC, CEPC, FCC-ee, etc. Figure 5 shows the possible future comparisons of the SM perditions and the the direct measurements [1].

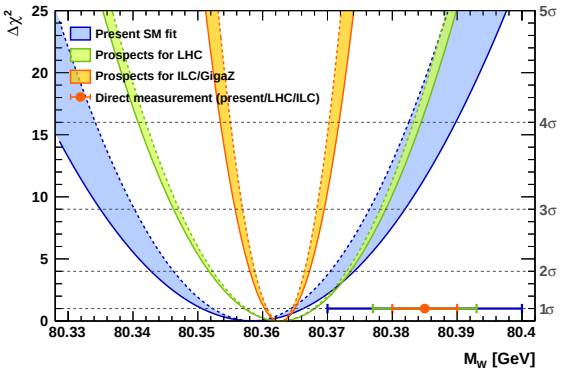

Figure 5: Comparison of the SM predicted M_W and directly measured M_W. In blue the present result, and in light blue, free and orange the present, LHC and ILC/GigaZ scenarios, repsctively.

References

[1] The Gfitter Group (http://cern.ch/gfitter), arXiv:1410.2299v1 [hep-ph] (2014).

[2] T. Aaltonen *et al.* (CDF Collaboration, D0 Collaboration), "Combination of CDF and D0 W-Boson mass measurements", Phys. Rev. D **88**, 052018, (2013).

[3] V. M. Abazov *et al.* (D0 Collaboration), Phys. Rev. Lett. **103**, 141801 (2009).

[4] V. M. Abazov *et al.* (D0 Collaboration), Phys. Rev. Lett. **108**, 151804 (2012).

[5] C. Amsler *et al.*, Phys. Lett. B **667**, 1 (2008) and references therein.

[6] C. Balazs and C. P. Yuan, Phys. Rev. D **56**, 5558 (1997).

[7] P. Golonka and Z. Was, Eur. Phys. J. C **45**, 97 (2006).

[8] P. M. Nadolsky, H. -L. Lai, Q. -H. Cao, J. Huston, J. Pumplin, D. Stump, W. -K. Tung, and C. -P. Yuan, Phys. Rev. D **78**, 013004 (2008).

[9] F. Landry, R. Brock, P. M. Nadolsky, and C. P. Yuan, Phys. Rev. D **67**, 073016 (2003).

[10] V. M. Abazov *et al.*, (D0 Collaboration), Phys. Rev. Lett. **100**, 102002 (2008).

[11] J. Alitti *et al.* (UA2 Collaboration), Phys. Lett. B **276**, 354 (1992).

[12] R. Brun and F. Carminati, CERN Program Library Long Writeup, Report No. W5013, (1993).

[13] T. Sjöstrand, S. Mrenna, and P. Skands, J. High Energy Phys. **05**, 026 (2006).

[14] H. L. Lai, J. Huston, S. Kuhlmann, F. Olness, J. Owens, D. Soper, W. K. Tung, and H. Weerts, Phys. Rev. D **55**, 1280 (1997); D. Stump, J. Huston, J. Pumplin, W. -K. Tung, H. -L. Lai, S. Kuhlmann, and J. F. Owens, J. High Energy Phys. **10**, 046 (2003).

[15] U. Baur, S. Keller, and D. Wackeroth, Phys. Rev. D **59**, 013002 (1998).

[16] U. Baur, S. Keller, and W. K. Sakumoto, Phys. Rev. D **57**, 199 (1998); U. Baur, O. Brein, W. Hollik, C. Schappacher, and D. Wackeroth, Phys. Rev. D **65**, 033007 (2002).

[17] L. Lyons, D. Gibout, and P. Clifford, Nucl. Instrum. Methods in Phys. Res. A **270**, 110 (1988); A. Valassi, Nucl. Instrum. Methods in Phys. Res. A **500**, 391 (2003).

[18] T. Aaltonen *et al.* (CDF Collaboration), Phys. Rev. Lett. **108**, 151803 (2012).

[19] P. Nason, JHEP 0411 (2004) 040; S. Frixione, P. Nason and C. Oleari, JHEP 0711 (2007) 070; S. Alioli, P. Nason, C. Oleari and E. Re, JHEP 1006 (2010) 043.

[20] L. Barze, G. Montagna, P. Nason, O. Nicrosini, F. Piccinini, arXiv:1202.0465 [hep-ph] (2012); L. Barze, G. Montagna, P. Nason, O. Nicrosini, F. Piccinini, A. Vicini, arXiv:1302.4606 [hep-ph] (2013).